Journal of Applied Physics

Acoustic emission study on avalanche dynamics of ferroelectric switching in lead zirconate titanate ceramics

Cite as: J. Appl. Phys. **132**, 224102 (2022); https://doi.org/10.1063/5.0126308
Submitted: 15 September 2022 • Accepted: 16 November 2022 • Published Online: 08 December 2022

Guomang Shao, Yangyang Xu, Yumei Zhou, et al.

AIP Publishing

Journal of Applied Physics ARTICLE scitation.org/journal/jap

Acoustic emission study on avalanche dynamics of ferroelectric switching in lead zirconate titanate ceramics

Cite as: J. Appl. Phys. **132**, 224102 (2022); doi: 10.1063/5.0126308
Submitted: 15 September 2022 · Accepted: 16 November 2022 ·
Published Online: 8 December 2022

Guomang Shao,[1] Yangyang Xu,[1] Yumei Zhou,[1,a)] Xiangdong Ding,[1] Jun Sun,[1] E. K. H. Salje,[1,2,a)] Turab Lookman,[3] and Dezhen Xue[1,a)]

AFFILIATIONS

[1]State Key Laboratory for Mechanical Behavior of Materials, Xian Jiaotong University, Xi'an 710049, China
[2]Department of Earth Sciences, Cambridge University, Downing Street, Cambridge CB2 3EQ, United Kingdom
[3]AiMaterials Research LLC, Santa Fe, New Mexico 87501, USA

[a)]**Authors to whom correspondence should be addressed:** zhouyumei@xjtu.edu.cn; ekhard@esc.cam.ac.uk; and xuedezhen@xjtu.edu.cn

ABSTRACT

The avalanche dynamics of ferroelectric switching in lead zirconate titanate ceramics was investigated using acoustic emission. Two distinct power-law regimes for ferroelectric switching events were identified by an anomaly in the histogram of probability density, in contrast to the single power-law behavior observed in $BaTiO_3$ single crystals. Such an anomaly is ascribed to the different minimum cut-offs of two power-law distributions. The critical energy exponents were determined to be 1.25 ± 0.10 for energies $<10^3$ aJ and 1.51 ± 0.14 for energies $>10^3$ aJ. The events in both regimes can be attributed to the depinning of domain walls from two distinct types of defects. The events in the lower energy regime are associated with domain wall junctions due to long-range electric and elastic interactions, whereas the latter is related to extrinsic defects, such as vacancies and dislocations. Moreover, for both regions, the rate of aftershocks follows the Omori power-law, indicating the same critical temporal correlations between the avalanches.

I. INTRODUCTION

Ferroelectric materials possess a large and switchable spontaneous polarization and have found numerous applications ranging from ultrasonic transducers and precision actuators to nonvolatile memories.[1–3] Spontaneous polarization is formed after a ferroelectric phase transition, which can produce complex domain patterns as a result of long-range electric and elastic interactions.[1,4] The polarizations can be switched to align along the field direction under large electric fields or mechanical stress. This is generally achieved via domain wall motion.[5–9]

The domain wall motion can be pinned by domain wall junctions (i.e., intersections of two domain walls) or point defects and then depinned after accumulation of adequate energy.[10–15] As a result, the continuous and smooth motion of domain walls is hindered, giving rise to "jerky" movements. Moreover, such domain wall motions always involve a large number of domains responding to the external field simultaneously.[10,14–17] The collective behavior of the "jerky" switching follows avalanche dynamics.[10,14–17] That is, the size (e.g., energy and amplitude) of individual switching events obeys a power-law, $P(S) \sim S^{-\varepsilon}F(S)$, where $P(S)$ is the probability density distribution (PDF) for the size and $F(S)$ is an exponential damping function.[15,18–22] Such a collective switching phenomenon has been incrementally studied in ferroelectric materials.[15] For example, Salje *et al.* have shown that the acoustic emission signals generated during ferroelectric switching in the $BaTiO_3$ single crystal follow a power-law distribution with an exponent ε of about 1.65.[17] Xu *et al.* have reported crystallographic anisotropy in the critical exponents for $BaTiO_3$ single crystals.[10] Casals *et al.* have analyzed the spatial distribution of avalanches in $BaTiO_3$ single crystals during the polarization switching process and showed that the energies, areas, and perimeters of the switched regions are all power-law distributed with exponents close to predicted mean field values.[14]

In practical applications, polycrystalline ceramics composed of a large number of differently oriented grains are more widely used due to their low cost and easy fabrication.[23] Many domains appear in each grain, and polarization within each domain orientates among the crystallographically allowable directions of the grain.[7] Upon application of an external field, the domains in one grain attempt to switch, similar to single crystals. However, the constraints from the neighboring grains and more abundant crystal defects will affect the collective process of polarization switching, resulting in different avalanche dynamics from that observed in ferroelectric single crystals.[7] Flannigan *et al.* measured electric currents during polarization switching of lead zirconate titanate (PZT) ceramics and reported critical exponents different from the results of single crystals.[24,25] Although the values of the exponents were obtained from electric signals for ceramics, they were determined from elastic signals of single crystals. The latter involves primarily 90° domains and *a priori* is not identical to the former ceramics.[4,16,17,24,25] Therefore, an acoustic emission (AE) measurement on a ceramic sample is needed to uncover the differences in avalanche dynamics of polarization switching between the ceramic and single crystal.

In the present study, we employed AE to monitor the polarization switching process in PZT ceramics, the current workhorse of ferroelectric materials. The AE technique is able to collect the acoustic waves due to sudden local strain changes within the sample.[26] The key advantage of AE is that it carries the whole temporal and spatial information of the acoustic source mechanism. This enables us to determine the energy and duration of avalanches and the waiting time between successive events.[27] In the histogram of probability density, an anomaly was observed around the energy of 10^3 aJ. The anomaly allows us to identify two distinct power-law regions for the ferroelectric switching of PZT, which is in contrast to the single power-law behavior observed in $BaTiO_3$ single crystals. The occurrence of the anomaly is ascribed to the different minimum cut-offs of two power-law distributions. The avalanche critical energy exponents were determined to be 1.25 ± 0.10 for energies less than 10^3 aJ and 1.51 ± 0.14 for energies greater than 10^3 aJ. For both regions, the rate of aftershocks follows the Omori power-law, indicating the same critical temporal correlations between the avalanches. The pinning effect of two distinct types of defects including domain wall junctions and extrinsic defects, such as vacancies and dislocations, is considered to be the origin of two distinct exponents.

II. EXPERIMENTAL DETAILS

The PZT ceramic sample with composition at the morphotropic phase boundary, $Pb(Zr_{0.52}Ti_{0.48})O_3$, was prepared by hot press sintering technology. A thin plate of the sample was polished and both surfaces of the sample were covered with silver to measure the ferroelectric hysteresis loops at 10 Hz. The experimental setup for the AE measurement is schematically shown in Fig. 1. The electric field was applied to the sample by a precision voltage source at a rate of ~0.4 kV/cm s. Experimental trials have shown that there are few acoustic signals under slow rates of applying an electric field, including 0.02, 0.1, and 0.2 kV/cm·s. The AE device was supplied by Vallen company (Germany). The piezoelectric

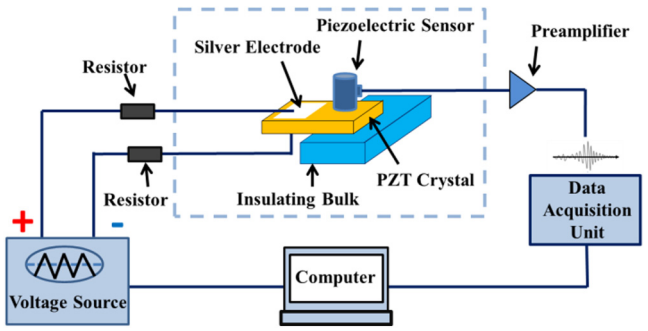

FIG. 1. Experimental setup for AE measurement.

sensor is encapsulated in stainless steel to reduce electrical noise and is acoustically coupled with the sample plates by a thin layer of vaseline. The acoustic signals were amplified by 34 dB, band filtered (between 95 and 850 kHz), and transferred to an acquisition system with a sampling frequency of 20 MHz. For suppressing the AE signals caused by sample vibration due to electrical coupling between the power supply and the piezoelectric sample, we inserted two resistors of 10 MΩ in the test circuit.[28] A threshold of 24.5 dB was set to identify jerky signals. An event begins when the signal intersects with the threshold and terminates when it is smaller than the threshold for more than 50 μs. The jerk amplitude is defined as the maximum voltage during the jerk signal. The energy was calculated by numerical integration of the squared voltage of signals during the interval, which gives the unit of 10^{-14} V·s^2. A resistance of 10 kΩ is used to scale the units of V s^2 to Joule, so that 10^{-14} V s^2 corresponds to 1 aJ. In order to exclude the possible influence from external noises, we measured the environmental noise without applying an electric field and in the presence of an electric field, which is achieved by replacing our sample with a non-ferroelectric insulator. The magnitude of the environmental noise is lower than 24.5 dB of our threshold, and thus, the environmental noises were filtered. Moreover, the upper limit of amplitude is 100 dB during the test as shown in Fig. S1 in the supplementary material, which is higher than all of our signals and indicates no truncation from the amplifier.

III. RESULTS AND DISCUSSION

A. Acoustic emission test

Figure 2(a) shows the polarization-electric field (P-E) hysteresis loop for PZT under an electric field of 21 kV/cm. The saturation polarization is about 30 μC/cm^2 and the coercive field value is about 7.59 kV/cm, consistent with values in literature.[29] The P-E hysteresis loop in Fig. 2(a) involves both 180° (ferroelectric) and 90° (ferroelastic) switching. Our AE measurements only detect signals from ferroelastic switching. Figure 2(b) shows the reconstructed hysteresis loop from the AE signals generated during a hysteresis loop. The loop (blue points) was obtained by integrating the energy of each avalanche signal (red points) over the applied electric field. It can be seen that the integrated avalanche energy

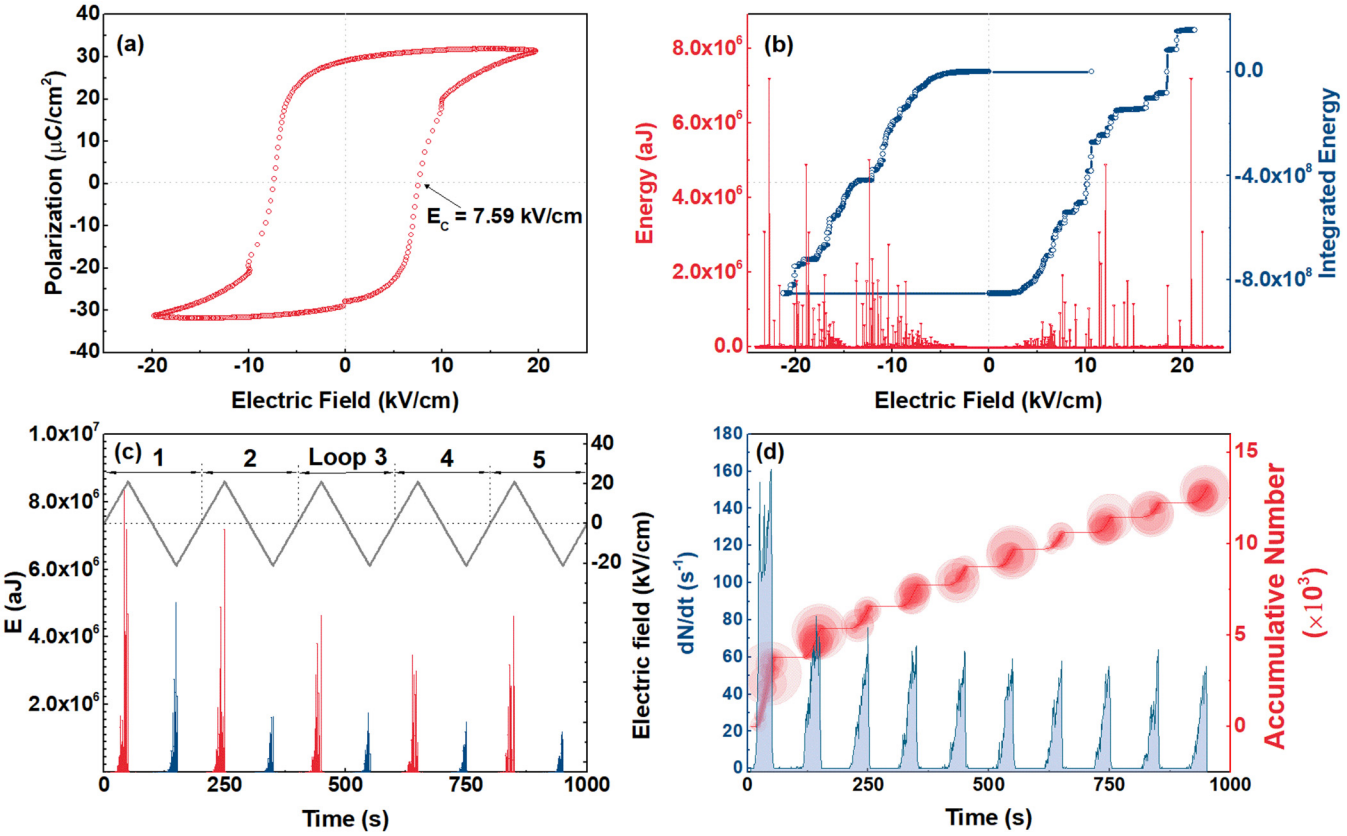

FIG. 2. (a) Polarization–electric field hysteresis. (b) AE energy (left axis) and the integrated energy (right axis) as a function of the electric field. (c) Spectrum of acoustic noise with a linear scale (red signal for positive loading and blue signal for negative loading). The electric field is ramped between −21 and 21 kV/cm with a rate of 20 V/s. (d) The AE activity (left axis) and the accumulated event number (right axis) as a function of time. The size of the circles depends on the AE energy (circle size ~E_{AE}).

reproduces the shape of hysteresis for PZT ceramic quite well and gives an approximative, consistent coercive field value. This suggests that the ferroelastic contribution plays an essential role in the electric field-driven switching process for PZT ceramics. Moreover, step-wise or jerky changes can be found in the reconstructed hysteresis loop, which is an electric analogy of Barkhausen noise in ferromagnetic materials.[30] The Barkhausen noise in ferroelectric materials contains the contribution from the elastic effect.

The AE signals generated during polarization switching over five periods of a triangular AC electric field were collected for the statistical analysis, and the spectrum is shown in Fig. 2(c). Figure 2(d) shows the accumulated number of signals, and the signal activity is defined as the number of acoustic signals per unit time. The size of the bubbles is proportional to the energy of the acoustic signals within each switching process. The peak of the acoustic signal activity appears near the coercive field of ±7.59 kV/cm. A decrease in both the energy of AE signals and the AE activity with the switching cycle number is noted, and the reason may be the reduction in the number of non-90° domains and degradation of the sample during cycling.

B. Statistical characteristics of AE signals

The PDFs of energy and amplitude of the AE signals during the switching process are shown in Figs. 3(a) and 3(c), respectively. On a log–log scale, the histogram of probability density should be a straight line for systems with a single power-law distribution. However, in our histograms of both energy and amplitude, a discontinuity or bump can be observed at an energy of 10^3 aJ and an amplitude of 10^3 μV. Such an anomaly separates the histogram into two linear regimes, suggesting that there presumably exist two exponents as shown by the triangles in Figs. 3(a) and 3(c). We then utilized the least squares method (LSM) to fit the histograms for the two regimes in Figs. 3(a) and 3(c). The avalanche critical energy exponents were determined to be 1.25 ± 0.10 for energies less than 10^3 aJ and 1.51 ± 0.14 for energies greater than 10^3 aJ. The former exponent 1.25 is the lower bound with error margins around 0.10. The exponent 1.25 is close to the critical value of 1.33 in the mean field theory and may be suppressed by the superposition with mild fluctuations which reduces the effective exponent.[11] Similarly, the two exponents obtained with the LSM method for amplitude distribution $p(A) \sim A^{-\tau}$ are $\tau = 1.49 \pm 0.11$

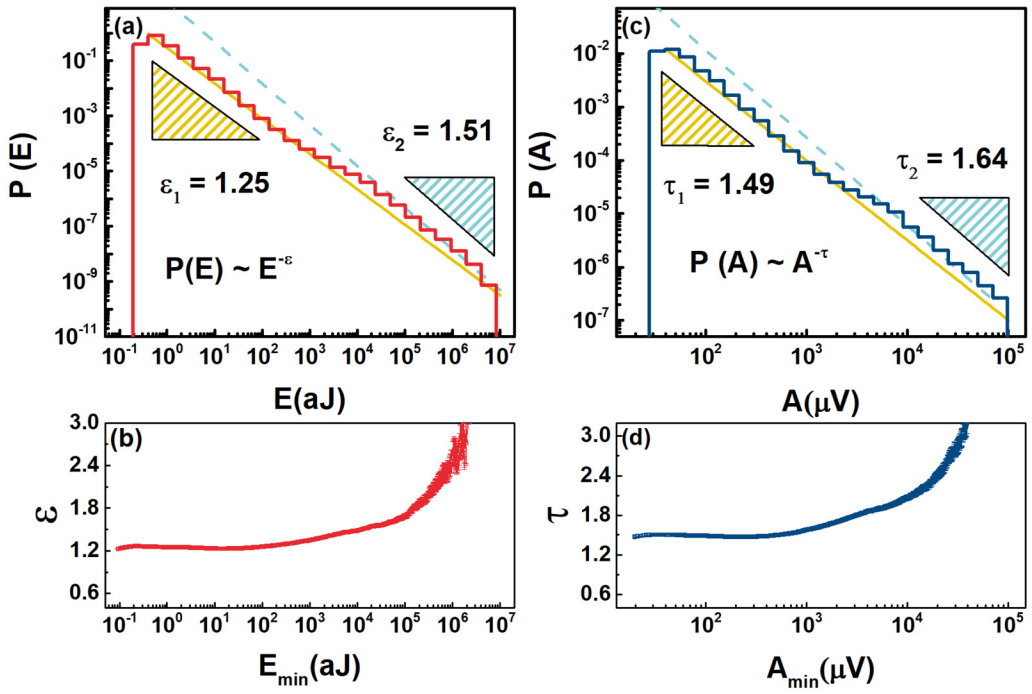

FIG. 3. (a) and (c) The probability distribution function of AE energy and amplitude. (b) and (d) The maximum likelihood method estimates for AE energy and amplitude.

and 1.64 ± 0.08. The exponent for the power-law distributions for $p(E) \sim E^{-}\varepsilon$ was usually estimated by the maximum likelihood (ML) method,[25,31] in which the likelihood function is the probability of a set of measurements $\{E_i\}$, defined as $L(\varepsilon) = \prod_{i=1}^{N} p(E_i)$. The estimate of $\varepsilon = \hat{\varepsilon}$ and $\tau = \hat{\tau}$ that maximizes the likelihood function is shown as a function of the lower limit of the energy $E_{\min}$ and the amplitude $A_{\min}$ in Figs. 3(b) and 3(d). The plateau in the ML estimation curve at the lower energy side corresponds to the lower exponent, whereas no obvious plateau appears for the higher energy side, which may be due to the existence of exponential damping.[32]

In the case of a mixture of two power-laws, one should expect a high exponent in the low energy region and a low exponent in the high energy region,[32] which is, however, in contrary to our experimental observations. Moreover, the existence of a discontinuity or bump in the histogram is unusual and of interest, as the reasons from the external environmental noise and the truncation of the amplifier can be excluded. In Sec. III C, we will discuss the reasons for the above anomalies.

C. Mixture of two power-law distributions with different minimum cut-offs

In some cases, the signals from two power-laws with different critical exponents may exhibit the same minimum cut-off, which gives a mixture of two power-laws and has been well modeled.[32] Here, we considered the situation that the minimum cutoff is different for two power-law distributions. The true probability density p(S) for such a mixture is given by

$$p(S) = \begin{cases} \left(\frac{\alpha-1}{S_{min.\alpha}^{1-\alpha}}\right) S^{-\alpha}, & S < S_{min.\beta}, \\ x(\alpha-1)\frac{S^{-\alpha}}{S_{min.\alpha}^{1-\alpha}} + (1-x)(\beta-1)\frac{S^{-\beta}}{S_{min.\beta}^{1-\beta}}, & S > S_{min.\beta}, \end{cases} \quad (1)$$

where $S_{min.\alpha}$ and $S_{min.\beta}$ are the two different minimum cutoffs of power-law distributions with critical exponents α and β, respectively. With the assumption that $S_{min.\alpha}$ is less than $S_{min.\beta}$, the signals with a size smaller than $S_{min.\beta}$ all come from the power-law distribution having exponent α. Thus, at a low energy range ($S < S_{min.\beta}$), a pure power-law can be observed. For the signals with a size larger than $S_{min.\beta}$, the fraction x comes from the power-law with an exponent α and the remaining fraction $1-x$ corresponds to a power-law with exponent β. Thereby, the high energy range ($S > S_{min.\beta}$) of signals follows a mixture of power-law. Such a model may explain the anomalies observed in our experiment.

Based on the model, we performed a study on different sets of synthetic data generated according to two power-law distributions with one of $S_{min.\alpha} = 0.1$ and $\alpha = 1.25$ and the other of $S_{min.\beta} = 1000$ and $\beta = 1.51$. The exponents were selected according to our experimental determined values, while the reason for $S_{min.\beta} = 1000$ is that the bump takes place at 10^3 aJ in our data. All the numerical

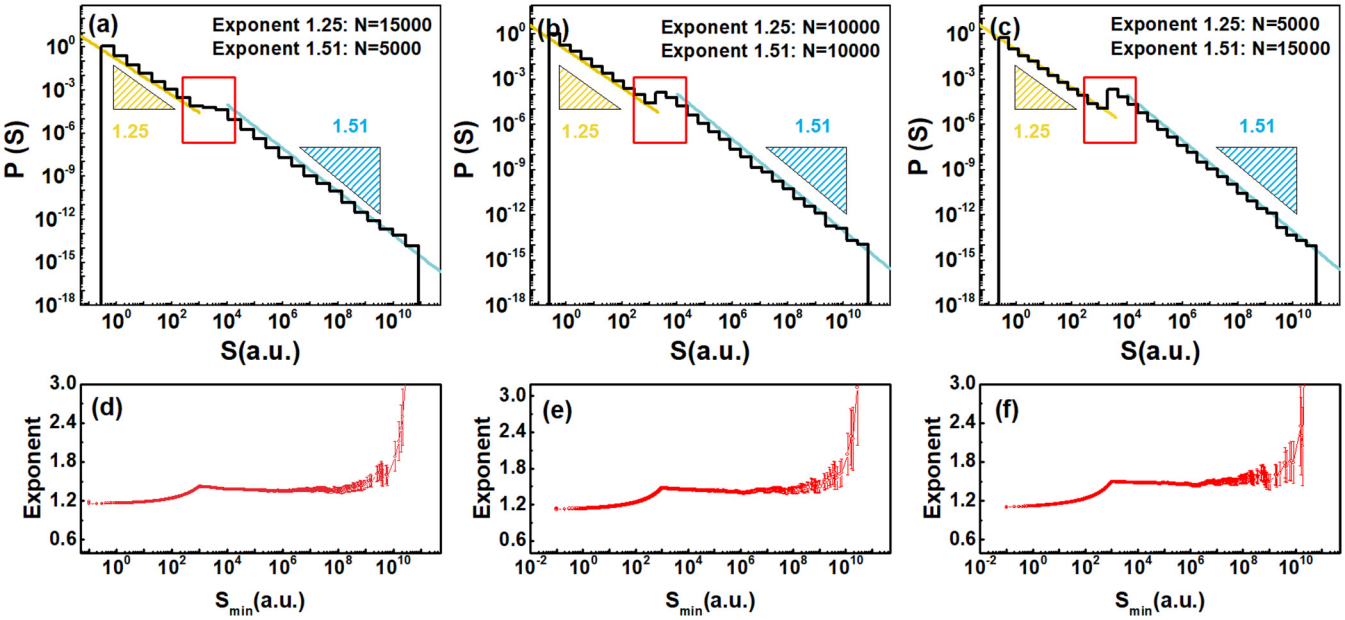

FIG. 4. PDFs and ML estimations of three typical sets of synthetic data, which possess a different ratio of numbers of signals, including (a) and (d) 75%–25%, (b) and (e) 50%–50%, and (c) and (f) 25%–75%. The data are generated according to two power-law distributions with one of $S_{min.\alpha} = 0.1$ and $\alpha = 1.25$ and the other of $S_{min.\beta} = 1000$ and $\beta = 1.51$.

samples were obtained by using the R package "poweRlaw" proposed by Gillespie *et al.*[31,33]

Figure 4 shows the PDFs and ML estimations of three typical sets of data, which possess a different ratio of numbers of signals, including 75%–25%, 50%–50%, and 25%–75% mixtures. In all three cases, an anomaly can be observed around 1000 in the histogram of probability density. It agrees with the minimum cutoff $S_{min.\beta}$ of a power-law distribution with an exponent of 1.51. Therefore, an anomaly can be observed for a system with two power law regimes with different exponents when the minimum cutoff S_{min} of the two power-law distributions is different. At which size the anomaly occurs is determined by the value of the minimum cutoff $S_{min.\beta}$. It is also observed that a larger portion of the signals from the power-law with a larger exponent results in a more obvious bump. Our experimental observation is similar to the situation shown in Fig. 4(a), indicating that the signals from the power-law distribution with a low exponent are dominant in our case. Though the high exponent part is actually a mixture of two power laws, the contribution from the other power-law distribution is quite small in our experimental signals so that a high exponent can be roughly determined.

D. Physical mechanism for the two different power-law distributions

The next question is what is the physical mechanism for the two different power-law distributions. We considered that both power-law distributions are due to the pinning–depinning of the domain wall to the pinning centers. Besides the intrinsic domain wall junctions due to long-range elastic and electric interactions, extrinsic defects, such as oxygen vacancies and dislocations, are also present in the PZT ceramic sample.[24,25,34] The two regions with different exponents likely correspond to the pinning effect of domain walls by the two types of disorder. Compared to intrinsic disorder, extrinsic defects cause larger local lattice distortions and local stress fields and, thus, produce a stronger pinning effect. More large events, thereby, could occur for the pinning–depinning to the point defects compared to the situation of domain wall junctions.[12] Therefore, a higher minimum cutoff S_{min} for the extrinsic defects is expected, while depinning from the domain wall junctions creates weaker AE signals and, thus, possesses a lower minimum cutoff S_{min}. Therefore, the lower energy exponent of 1.25 may be ascribed to the weaker pinning effect by the intrinsic disorder. The larger

TABLE I. Comparison of energy exponents for PZT ceramics and $BaTiO_3$ single crystals generated from electrical and acoustic signal sources.

Signal	Sample	Region I intrinsic disorder	Region II extrinsic disorder	Ref.
Electrical	PZT ceramic	1.79 ± 0.08[a]	2.04 ± 0.19[a]	25
Acoustic	PZT ceramic	1.25 ± 0.10	1.51 ± 0.14	Present work
Acoustic	BTO single crystal	1.65 ± 0.10	…	17

[a]Although the authors did not identify, our model suggests that 1.79 is for intrinsic disorder and 2.04 is for extrinsic disorder.

energy exponent 1.51 is due to the stronger pinning centers associated with extrinsic defects. A similar phenomenon was reported in a previous study by Flannigan *et al.*,[25] who also found a low exponent in the low energy region and a high exponent in the high energy region for the electric signals of PZT ceramics. As shown in Table I, the exponents from electric signals are larger than those obtained from AE measurements, which indicate that the former signals originate from both 90° and non-90° domain switching. The single power-law distribution of avalanche events in single crystal $BaTiO_3$ is primarily due to intrinsic disorder.[17]

E. Scaling relationship

During ferroelectric polarization switching, the energy (E), amplitude (A), and duration (D) are statistically related through $E \sim A^x$ and $A \sim D^\chi$. Figure 5(a) shows the correlation between E and A, which yields $x = 1.97 \pm 0.01$ estimated by the least squares method. Figure 5(b) gives A vs density D of the AE signals. In the log–log plot, D is approximately linear with the amplitude A when $D > 50\,\mu s$. The exponent χ was estimated to be 2.55 ± 0.09. We note that the scale invariant relationship $(\varepsilon - 1)x = (\tau - 1)$ is satisfied by those exponents. For the lower value region with

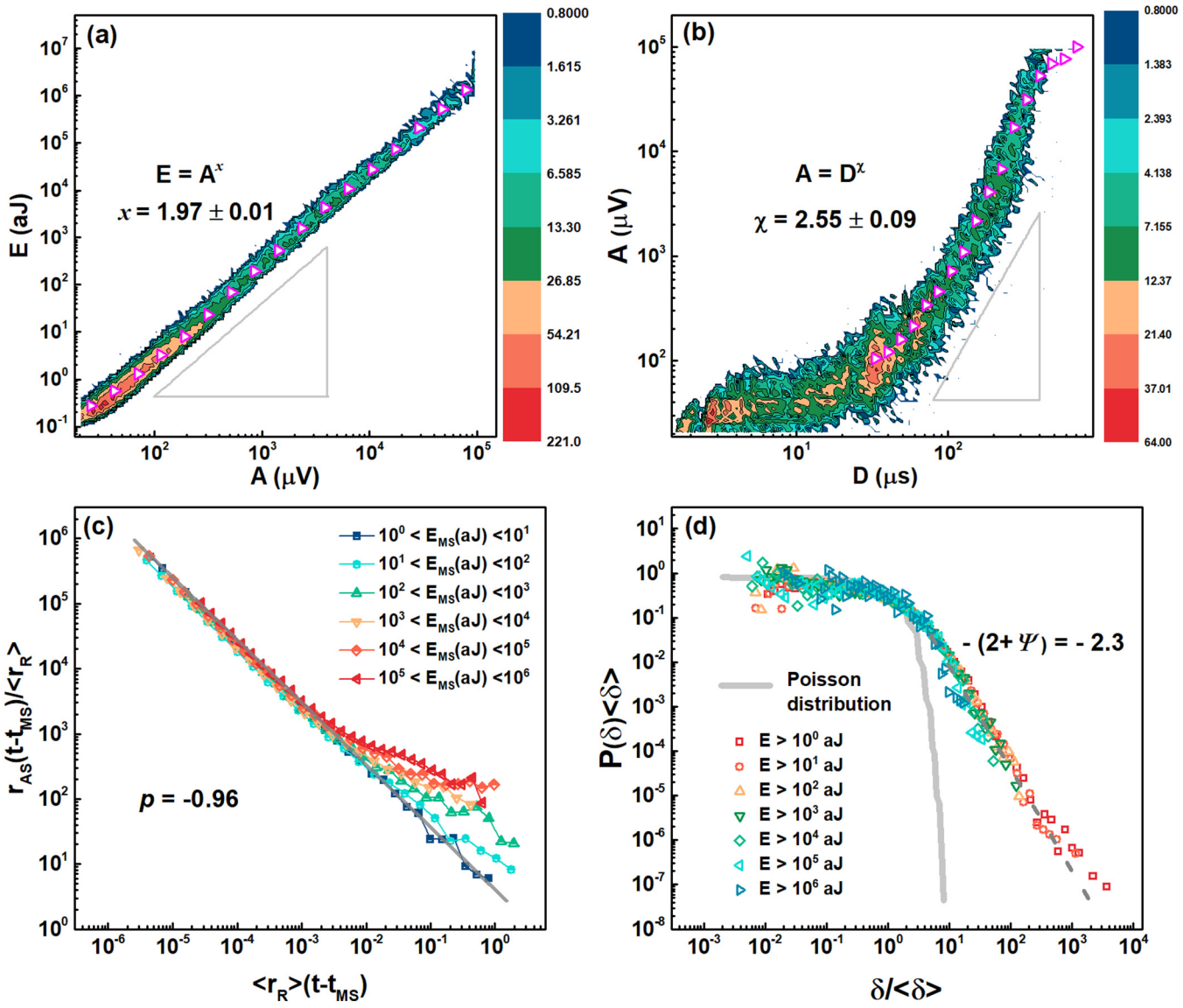

FIG. 5. The correlation (a) between the energy and the amplitude and (b) between the amplitude and the duration. (c) Rate of aftershocks per unit time, r, as a function of the time lapse to the main shock. (d) Scaled waiting time for events between adjacent events for small and large waiting times.

$\tau = 1.49 \pm 0.11$ and $\varepsilon = 1.25 \pm 0.10$, $(\varepsilon - 1)x = (\tau - 1) \approx 0.5$. For larger values of the two segments, $\tau - 1 = 0.64$ and $(\varepsilon - 1)x = 1.00$, which suggests that they are roughly equal within experimental uncertainties. The power-law distribution of energies and amplitudes and the scaling relationship between exponents indicate that the evolution of ferroelectric domains driven by an electric field takes place in the absence of a characteristic size, which is a typical feature of criticality.[35]

F. Temporal correlation of AE signals

Finally, we performed an aftershock analysis to investigate the temporal correlations between avalanche events during polarization switching. That is, the subsequent small signals are induced by the main-shocks (MSs, i.e., large signals). MSs are defined as signals whose energies are within a predefined energy range. The signals whose energy is lower than a MS and occur after the MS are defined as aftershocks (ASs). The time is normalized through a time lag from each AS to its MS, defined as $t - t_{MS}$. A sequence of energy ranges is employed to define MS and corresponding AS. A rescaled rate of AS (r_{AS}) defined by the number of AS within a unit time for all the MS is known to follow the Omori law,[36–40]

$$r_{AS}\,(t - t_{MS}) = (c - t - t_{MS})^{-p}, \tag{2}$$

where c is the constant independent of time, p is the critical exponent near 1 for earthquakes and other materials.[38,41] Figure 5(c) shows that the Omori law is satisfied by the present AE signals for times shorter than 0.01 s and deviations occur for longer times. This indicates that the events occurring shortly after a mainshock are strongly correlated, whereas later events are not.

The distribution of waiting times between adjacent signals ($\delta_n = t_{n+1} - t_n$) further supports the presence of temporal correlations of polarization switching events. The PDF of waiting times, $p(\delta)$, can be expressed as $p(\delta) = \frac{1}{\langle\delta\rangle}\Phi\left(\frac{\delta}{\langle\delta\rangle}\right)$, where $\langle\delta\rangle$ is the mean value of waiting time, and the analytical expression for the scaling function Φ is assumed to follow[42,43]

$$\Phi(x) = \begin{cases} x^{-(1-\nu)} & x \ll 1, \\ x^{-(2+\Psi)} & x \gg 1. \end{cases} \tag{3}$$

Different threshold values in energy were selected to filter the data with lower energies. Although the scaled waiting time should follow double power-law distributions as shown in Eq. (3), the PZT ceramic possesses one region for times longer than 1 s with exponent $(2 + \Psi) = 2.3$ as shown in Fig. 5(d). For times shorter than 1 s, the waiting time follows a Poisson distribution. The reason for the absence of the lower time branch is that the loading rate in the present study is too high so that signals may overlap.

IV. SUMMARY

In summary, we have studied the avalanche dynamics of ferroelectric switching in lead zirconate titanate (PZT) ceramics by AE measurements. Our results show that ferroelectric switching in PZT ceramics follows a power-law distribution in different energy regimes with exponent $\varepsilon = 1.25 \pm 0.10$ for energies less than 10^3 aJ and $\varepsilon = 1.51 \pm 0.14$ for energies greater than 10^3 aJ. The superposition of power-laws is consistent with the results measured electrically.[25] We suggest that the two energy exponents can be attributed to the pinning effect of the domain walls by the extrinsic disorder of point defects and dislocations as well as the intrinsic disorder of domain wall junctions. We also find that the rate of aftershocks decays as a function of the time interval to the main shock as per the Omori-like power-law distribution, suggesting that critical temporal correlations exist between avalanches during ferroelectric switching in PZT.

SUPPLEMENTARY MATERIAL

See the supplementary material for the relationship between amplitude and time of the signal around the observed bump (10^3–10^5 aJ).

ACKNOWLEDGMENTS

The authors gratefully acknowledge the support of the National Key Research and Development Program of China (No. 2021YFB3802102), the National Natural Science Foundation of China (NNSFC) (Grant Nos. 52173228 and 51931004), and the 111 project 2.0 (No. BP2018008). E.K.H.S is grateful to EPSRC (No. EP/P024904/1). The project has received funding from the EU's Horizon 2020 programme under the Marie Skłodowska-Curie Grant Agreement No 861153.

AUTHOR DECLARATIONS

Conflict of Interest

The authors have no conflict to disclose.

Author Contributions

Guomang Shao and Yangyang Xu contributed equally to this study.

Guomang Shao: Conceptualization (equal); Data curation (equal); Investigation (equal); Validation (equal); Writing – original draft (equal). **Yangyang Xu:** Conceptualization (equal); Data curation (equal); Investigation (equal); Validation (equal); Writing – original draft (equal). **Yumei Zhou:** Conceptualization (equal); Data curation (equal); Investigation (equal); Validation (equal); Writing – original draft (equal). **Xiangdong Ding:** Writing – review & editing (equal). **Jun Sun:** Writing – review & editing (equal). **E. K. H. Salje:** Conceptualization (equal); Data curation (equal); Investigation (equal); Validation (equal); Writing – original draft (equal). **Turab Lookman:** Writing – review & editing (equal). **Dezhen Xue:** Conceptualization (equal); Data curation (equal); Investigation (equal); Validation (equal); Writing – original draft (equal).

DATA AVAILABILITY

The data that support the findings of this study are available from the corresponding authors upon reasonable request.

REFERENCES

[1]M. E. Lines and A. M. Glass, *Principles and Applications of Ferroelectrics and Related Materials* (Oxford University, Oxford, 2001).
[2]K. Uchino, *Ferroelectric Devices*, 2nd ed. (CRC, Boca Raton, 2010).
[3]J. F. Scott, "Applications of modern ferroelectrics," Science **315**, 954 (2007).
[4]E. K. H. Salje, *Phase Transitions in Ferroelastic and Co-Elastic Crystals* (Cambridge University, Cambridge, 1991).
[5]C. T. Nelson, P. Gao, J. R. Jokisaari, C. Heikes, C. Adamo, A. Melville, S. H. Baek, C. M. Folkman, B. Winchester, Y. Gu, Y. Liu, K. Zhang, E. Wang, J. Li, L. Q. Chen, C. B. Eom, D. G. Schlom, and X. Pan, "Domain dynamics during ferroelectric switching," Science **334**, 968 (2011).
[6]W. J. Merz, "Piezoelectric ceramics," Nature **236**, 245 (1972).
[7]J. Y. Li, R. C. Rogan, E. Üstündag, and K. Bhattacharya, "Domain switching in polycrystalline ferroelectric ceramics," Nat. Mater. **4**, 776 (2005).
[8]P. Gao, C. T. Nelson, J. R. Jokisaari, S. H. Baek, C. W. Bark, Y. Zhang, E. Wang, D. G. Schlom, C. B. Eom, and X. Pan, "Revealing the role of defects in ferroelectric switching with atomic resolution," Nat. Commun. **2**, 591 (2011).
[9]A. R. Akhmatkhanov, I. A. Kipenko, A. A. Esin, and V. Y. Shur, "Barkhausen pulses caused by domain merging in congruent lithium niobate," Appl. Phys. Lett. **117**, 022903 (2020).
[10]Y. Xu, Y. Zhou, D. Xue, X. Ding, J. Sun, and E. K. H. Salje, "Anisotropic avalanche dynamics during ferroelectric switching in $BaTiO_3$ and $0.7Pb(Mg_{2/3}Nb_{1/3})O_3$–$0.3PbTiO_3$," Appl. Phys. Lett. **117**, 172901 (2020).
[11]E. K. H. Salje, "Mild and wild ferroelectrics and their potential role in neuromorphic computation," APL Mater. **9**, 010903 (2021).
[12]X. He, S. Li, X. Ding, J. Sun, S. M. Selbach, and E. K. H. Salje, "The interaction between vacancies and twin walls, junctions, and kinks, and their mechanical properties in ferroelastic materials," Acta Mater. **178**, 26–35 (2019).
[13]Y. Yang, L. Zhang, S. Li, X. Ding, J. Sun, J. Weiss, and E. K. H. Salje, "Mild fluctuations in ferroelastic domain switching," Phys. Rev. B **104**, 214103 (2021).
[14]B. Casals, G. F. Nataf, and E. K. H. Salje, "Avalanche criticality during ferroelectric/ferroelastic switching," Nat. Commun. **12**, 345 (2021).
[15]G. F. Nataf and E. K. H. Salje, "Avalanches in ferroelectric, ferroelastic and coelastic materials: Phase transition, domain switching and propagation," Ferroelectrics **569**, 82 (2020).
[16]G. F. Nataf, M. Guennou, J. M. Gregg, D. Meier, J. Hlinka, E. K. H. Salje, and J. Kreisel, "Domain-wall engineering and topological defects in ferroelectric and ferroelastic materials," Nat. Rev. Phys. **2**, 634 (2020).
[17]E. K. H. Salje, D. Xue, X. Ding, K. A. Dahmen, and J. F. Scott, "Ferroelectric switching and scale invariant avalanches in $BaTiO_3$," Phys. Rev. Mater. **3**, 014415 (2019).
[18]E. K. H. Salje and K. A. Dahmen, "Crackling noise in disordered materials," Annu. Rev. Condens. Matter Phys. **5**, 233 (2014).
[19]R. Niemann, J. Baró, O. Heczko, L. Schultz, S. Fähler, E. Vives, L. Mañosa, and A. Planes, "Tuning avalanche criticality: Acoustic emission during the martensitic transformation of a compressed Ni-Mn-Ga single crystal," Phys. Rev. B **86**, 214101 (2012).
[20]M. C. Gallardo, J. Manchado, F. J. Romero, and J. del Cerro, "Avalanche criticality in the martensitic transition of $Cu_{67.64}Zn_{16.71}Al_{15.65}$ shape-memory alloy: A calorimetric and acoustic emission study," Phys. Rev. B **81**, 174102 (2010).
[21]C. C. Vu, D. Amitrano, O. Plé, and J. Weiss, "Compressive failure as a critical transition: Experimental evidence and mapping onto the universality class of depinning," Phys. Rev. Lett. **122**, 015502 (2019).
[22]C. C. Vu and J. Weiss, "Asymmetric damage avalanche shape in quasibrittle materials and subavalanche (aftershock) clusters," Phys. Rev. Lett. **125**, 105502 (2020).
[23]P. K. Panda and B. Sahoo, "PZT to lead free piezo ceramics: A review," Ferroelectrics **474**, 128 (2015).
[24]C. D. Tan, C. Flannigan, J. Gardner, F. D. Morrison, E. K. H. Salje, and J. F. Scott, "Electrical studies of barkhausen switching noise in ferroelectric PZT: Critical exponents and temperature dependence," Phys. Rev. Mater. **3**, 034402 (2019).
[25]C. Flannigan, C. D. Tan, and J. F. Scott, "Electrical studies of Barkhausen switching noise in ferroelectric lead zirconate titanate (PZT) and $BaTiO_3$: Critical exponents and temperature- dependence," J. Phys.: Condens. Matter **32**, 055403 (2020).
[26]B. Ludwig, C. Strothkaemper, U. Klemradt, X. Moya, L. Mañosa, E. Vives, and A. Planes, "An acoustic emission study of the effect of a magnetic field on the martensitic transition in Ni2MnGa," Appl. Phys. Lett. **94**, 121901 (2009).
[27]E. K. H. Salje, E. Dul'kin, and M. Roth, "Acoustic emission during the ferroelectric transition to P4mm in $BaTiO_3$ and the ferroelastic transition in $Pb_3(PO_4)_2$," Appl. Phys. Lett. **106**, 152903 (2015).
[28]H. Aburatani, J. P. Witham, and K. Uchino, "A fractal analysis on domain related electric field induced acoustic emission in ferroelectric ceramics," Jpn. J. Appl. Phys. **37**, 602 (1998).
[29]N. Kumari, S. Monga, M. Arif, N. Sharma, A. Sanger, A. Singh, P. M. Vilarinho, V. Gupta, K. Sreenivas, R. S. Katiyar, and J. F. Scott, "Multifunctional behavior of acceptor-cation substitution at higher doping concentration in PZT ceramics," Ceram. Int. **45**, 12716 (2019).
[30]T. Le Manh, F. Caleyo, J. M. Hallen, J. A. Pérez Benítez, and J. H. Espina Hernández, "Novel method for the accurate determination of magnetocrystalline energy from barkhausen noise in ferromagnetic materials," Mater. Sci. Eng. B **225**, 98 (2017).
[31]A. Clauset, C. R. Shalizi, and M. E. J. Newman, "Power-law distributions in empirical data," SIAM Rev. **51**, 661 (2009).
[32]E. K. H. Salje, A. Planes, and E. Vives, "Analysis of crackling noise using the maximum-likelihood method: Power-law mixing and exponential damping," Phys. Rev. E **96**, 042122 (2017).
[33]C. S. Gillespie, "Fitting heavy tailed distributions: The poweRlaw package," J. Stat. Softw. **64**(2), 1–16 (2015).
[34]E. K. H. Salje, A. Saxena, and A. Planes, *Avalanches in Functional Materials and Geophysics* (Springer International Publishing, 2017).
[35]A. Planes, L. Mañosa, and E. Vives, "Acoustic emission in martensitic transformations," J. Alloys Compd. **577**, S699–S704 (2013).
[36]Y. Xu, A. G. Borrego, A. Planes, X. Ding, and E. Vives, "Criticality in failure under compression: Acoustic emission study of coal and charcoal with different microstructures," Phys. Rev. E. **99**, 033001 (2019).
[37]J. Baró, Á. Corral, X. Illa, A. Planes, E. K. H. Salje, W. Schranz, D. E. S. Parra, and E. Vives, "Statistical similarity between the compression of a porous material and earthquakes," Phys. Rev. Lett. **110**, 088702 (2013).
[38]T. Utsu, Y. Ogata, and R. S. Matsu'ura, "The centenary of the omori formula for a decay law of aftershock activity," J. Phys. Earth **43**, 1 (1995).
[39]Á. Corral and K. Christensen, "Comment on 'earthquakes descaled: On waiting time distributions and scaling laws,'" Phys. Rev. Lett. **96**, 109801 (2006).
[40]Á. Corral, "Long-term clustering, scaling, and universality in the temporal occurrence of earthquakes," Phys. Rev. Lett. **92**, 108501 (2004).
[41]Y. Xu, D. Xue, Y. Zhou, T. Su, X. Ding, J. Sun, and E. K. H. Salje, "Avalanche dynamics of ferroelectric phase transitions in $BaTiO_3$ and $0.7Pb(Mg_{2/3}Nb_{1/3})O_3$–$0.3PbTiO_3$ single crystals," Appl. Phys. Lett. **115**, 022901 (2019).
[42]P. Bak, K. Christensen, L. Danon, and T. Scanlon, "Unified scaling law for earthquakes," Phys. Rev. Lett. **88**, 178501 (2002).
[43]Á Corral, "Local distributions and rate fluctuations in a unified scaling law for earthquakes," Phys. Rev. E **68**, 035102 (2003).